Online Inductance Identification for PMSM Sensorless Control Immune to Position Error

Jiqing Xue[1], Qiwei Wang[1], Gaolin Wang[1], Guoqiang Zhang[1], and Dianguo Xu[1]
[1] Harbin Institute of Technology, China

***Abstract*-- The accuracy of position sensorless control depends largely on the permanent magnet synchronous motor (PMSM) inductance. Meanwhile, the PMSM inductance identification methods require the accurate rotor position. In position sensorless control, there is generally an angle deviation between the observed rotor position and the real rotor position, which will lead to error in PMSM parameters identification. In this paper, a relative rotation axis system and its high-frequency (HF) equivalent impedance model are proposed, in which the PMSM inductance identification and the rotor position error are decoupled. Therefore, by injecting the HF voltage signal, the PMSM inductance in position sensorless control can be accurately identified, which is immune to the rotor position error in position sensorless control. The experimental results show the effectiveness of the proposed PMSM inductance online identification method under different operation conditions.**

***Index Terms*-- online inductance identification, permanent magnet synchronous motor (PMSM), position sensorless control, relative rotation axis.**

I. Introduction

Permanent magnet synchronous motor (PMSM) has been widely used in electric vehicle, aerospace and other fields due to its superior speed regulation performance and high power-density [1]-[4]. In order to obtain the accurate control performance while reducing financial consumption, the PMSM position sensorless control methods have developed in recent decades [5]-[7]. During the online motor operation, the PMSM inductance changes due to the saturation effect [8]. Thus, a coupling problem is shown: the rotor position estimation error generally exists since the PMSM inductance is assumed to be constant in the general used position sensorless control strategies, but the accurate rotor position is required for the conventional PMSM inductance identification methods [9][10]. Hence, it is necessary to identify the PMSM inductance during motor operation.

Some PMSM position sensorless control methods consider parameters identification synchronously, and combine the two processes to improve the real-time control accuracy [11]. The online PMSM inductance identification is mostly based on voltage equations, which are generally rank-deficient. To solve the problem of rank deficiency, the most common method is introducing specific parameters obtained in advance [12][13]. It is a relatively easy way to make the model full-rank by introducing specific parameters, but the assumption of constant parameters during motor operation is inconsistent with the physical state. To make the model full-rank, signal injection is another commonly used method [14]-[16]. However, the traditional methods of PMSM parameters identification are mostly based on the accurate rotor position, which do not fully consider the rotor position error caused by the cross-coupling effect or the observation in position sensorless control. Therefore, it is of high practical value to propose an online inductance identification method immune to the rotor position error.

In order to avoid the coupling of the position sensorless control error and the PMSM inductance variation, an online inductance identification method based on the relative rotation axis system and its high-frequency (HF) equivalent impedance model is proposed, which is immune to the rotor position error in position sensorless control. This paper is organized as follows: the analysis of inductance identification and position error coupling in position sensorless control is proposed in section II. A relative rotation axis system and its HF equivalent impedance model of PMSM are proposed in section III. An online PMSM inductance identification method immune to the position error is proposed in section IV. The experimental results of the PMSM inductance identification are shown in section V.

II. Analysis of Inductance and Position Error Coupling Effect in Position Sensorless Control

The traditional position sensorless control of PMSM is mostly based on the Extended Counter-electromotive force (EEMF) equations, which can be expressed as

$$\begin{bmatrix} u_\alpha \\ u_\beta \end{bmatrix} = \begin{bmatrix} R_s + pL_d & \omega_e(L_d - L_q) \\ -\omega_e(L_d - L_q) & R_s + pL_d \end{bmatrix} \begin{bmatrix} i_\alpha \\ i_\beta \end{bmatrix} + \begin{bmatrix} e_{EEMF\alpha} \\ e_{EEMF\beta} \end{bmatrix} \quad (1)$$

$$\begin{bmatrix} e_{EEMF\alpha} \\ e_{EEMF\beta} \end{bmatrix} = \left[(L_d - L_q)(\omega_e i_d - p i_q) + \omega_e \lambda \right] \begin{bmatrix} -\sin\theta_e \\ \cos\theta_e \end{bmatrix} \quad (2)$$

where $u_{\alpha,\beta}$, $i_{\alpha,\beta}$, $e_{EEMF\alpha,\beta}$ are the α-β axis voltages, currents, and EEMFs respectively, $L_{d,q}$ are the d-q axis inductances, R_s is the stator resistance, p is the differential operator, ω_e is the electrical angular frequency, λ is the rotor flux linkage, θ_e is the rotor position. When only considering the impact of the PMSM inductance change during motor operation, the d-q axis inductance values in the EEMF equations deviate from the actual values, which can be expressed as

$$\begin{bmatrix} L_{do} \\ L_{qo} \end{bmatrix} = \begin{bmatrix} L_d + \Delta L_d \\ L_q + \Delta L_q \end{bmatrix} \quad (3)$$

where $L_{do,qo}$ are the d-q axis inductances in position sensorless observer, $\Delta L_{d,q}$ are the differences. Based on the above analysis, (1)-(2) need to be modified in position sensorless control, which are rewritten as

$$\begin{bmatrix} u_\alpha \\ u_\beta \end{bmatrix} = \begin{bmatrix} R_s + pL_{do} & \hat{\omega}_e(L_{do} - L_{qo}) \\ -\hat{\omega}_e(L_{do} - L_{qo}) & R_s + pL_{do} \end{bmatrix} \begin{bmatrix} i_\alpha \\ i_\beta \end{bmatrix} + \begin{bmatrix} \hat{e}_{EEMF\alpha} \\ \hat{e}_{EEMF\beta} \end{bmatrix} \tag{4}$$

$$\begin{bmatrix} \hat{e}_{EEMF\alpha} \\ \hat{e}_{EEMF\beta} \end{bmatrix} = \left[(L_{do} - L_{qo})(\hat{\omega}_e i_d - p i_q) + \hat{\omega}_e \lambda \right] \begin{bmatrix} -\sin\hat{\theta}_e \\ \cos\hat{\theta}_e \end{bmatrix} \tag{5}$$

where $\hat{\theta}_e$, $\hat{\omega}_e$, and $\hat{e}_{EEMF\alpha,\beta}$ are the rotor position, electrical angular frequency, and EEMFs in position sensorless control respectively. It can be seen from (1)-(5) that the observed rotor position in position sensorless control changes with the PMSM inductance. Thus, during the PMSM operation, the observed rotor position error in position sensorless control exists, due to the PMSM inductance deviation in observer.

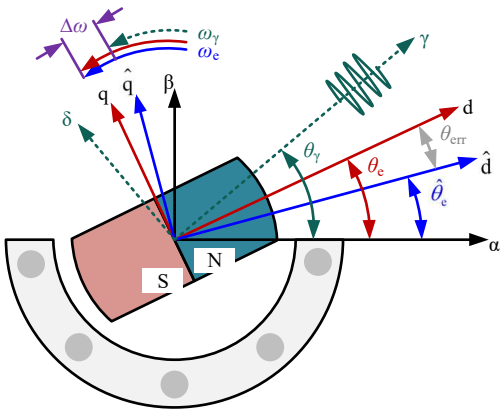

Fig. 1. Several axes of PMSM.

As is shown in Fig. 1, d-q axis represents the actual rotor position, $\hat{d}$-$\hat{q}$ axis represents the observed rotor position in position sensorless control, θ_{err} is the difference between θ_e and $\hat{\theta}_e$. The traditional PMSM inductance identification method based on d-q axis HF injection can be expressed as

$$\begin{bmatrix} u_{dh} \\ u_{qh} \end{bmatrix} = \omega_h \begin{bmatrix} L_d & 0 \\ 0 & L_q \end{bmatrix} \begin{bmatrix} i_{dh} \\ i_{qh} \end{bmatrix} \tag{6}$$

where $u_{dh,qh}$, $i_{dh,qh}$ are the d-q axis HF voltages and currents respectively, ω_e is the angular frequency of HF signals.

Due to the rotor position error in position sensorless control, the control and external injection signals are input into $\hat{d}$-$\hat{q}$ axis, so (6) need to be transformed into

$$\begin{bmatrix} u_{\hat{d}h} \\ u_{\hat{q}h} \end{bmatrix} = C_{err} \begin{bmatrix} u_{dh} \\ u_{qh} \end{bmatrix} = \omega_h C_{err} \begin{bmatrix} L_d & 0 \\ 0 & L_q \end{bmatrix} C_{err}^{-1} \begin{bmatrix} i_{\hat{d}h} \\ i_{\hat{q}h} \end{bmatrix} \tag{7}$$

$$C_{err} = \begin{bmatrix} \cos\theta_{err} & -\sin\theta_{err} \\ \sin\theta_{err} & \cos\theta_{err} \end{bmatrix} \tag{8}$$

where $\hat{u}_{dh,qh}$, $\hat{i}_{dh,qh}$ are the $\hat{d}$-$\hat{q}$ axis HF voltages and currents respectively, C_{err} is the coordinate transformation matrix generated due to the rotor position error. According to the impedance model, the results of the traditional PMSM inductance identification method based on HF injection can be expressed as

$$\begin{bmatrix} \hat{L}_d \\ \hat{L}_q \end{bmatrix} = \begin{bmatrix} \cos^2\theta_{err} & \sin^2\theta_{err} \\ \sin^2\theta_{err} & \cos^2\theta_{err} \end{bmatrix} \begin{bmatrix} L_d \\ L_q \end{bmatrix} \tag{9}$$

where $\hat{L}_{d,q}$ are the results of the PMSM inductance identification. It can be seen from (9) that the PMSM inductance identification values are not equal to their actual values due to the rotor position error in position sensorless control.

In summary, the coupling problem between the rotor position error and the PMSM inductance change in position sensorless control can be expressed as: the PMSM inductance deviation in observer can lead to the error of the observed rotor position, and the error of the observed rotor position can also have a negative impact on the PMSM inductance identification.

III. Relative Rotation Axis System and HF Equivalent Impedance Model

In order to decouple the rotor position error and the PMSM inductance, a relative rotation γ-δ axis system is constructed, as is shown in Fig. 1. The voltage equations in γ-δ axis can be transformed from that in abc-axis, which can be expressed as

$$\begin{aligned} \boldsymbol{u}_{\gamma\delta0} &= C_{abc/\gamma\delta0}\boldsymbol{u}_{abc} \\ &= C_{abc/\gamma\delta0}\left(p\boldsymbol{L}_{abc}\boldsymbol{i}_{abc}\right) + C_{abc/\gamma\delta0}\boldsymbol{R}_s\boldsymbol{i}_{abc} \\ &= p\left(C_{abc/\gamma\delta0}\boldsymbol{L}_{abc}C^{-1}{}_{abc/\gamma\delta0}\boldsymbol{i}_{\gamma\delta0}\right) - C_{abc/\gamma\delta0}\boldsymbol{R}_s C^{-1}{}_{abc/\gamma\delta0}\boldsymbol{i}_{\gamma\delta0} \end{aligned} \tag{10}$$

$$C_{abc/\gamma\delta0} = \frac{2}{3}\begin{bmatrix} \cos\theta_\gamma & \cos(\theta_\gamma - \frac{2\pi}{3}) & \cos(\theta_\gamma + \frac{2\pi}{3}) \\ -\sin\theta_\gamma & -\sin(\theta_\gamma - \frac{2\pi}{3}) & -\sin(\theta_\gamma + \frac{2\pi}{3}) \\ \frac{1}{2} & \frac{1}{2} & \frac{1}{2} \end{bmatrix} \tag{11}$$

where $C_{abc/\gamma\delta0}$ is the coordinate transformation matrix from abc-axis to γ-δ axis, θ_γ is the position of γ-δ axis. According to (10), the resistance and the γ-δ axis inductances can be expressed as

$$\begin{cases} \boldsymbol{R}_{\gamma\delta0} = C_{abc/\gamma\delta0}\boldsymbol{R}_s C^{-1}{}_{abc/\gamma\delta0} = \boldsymbol{R}_s \\ \boldsymbol{L}_{\gamma\delta0} = C_{abc/\gamma\delta0}\boldsymbol{L}_{abc}C^{-1}{}_{abc/\gamma\delta0} \end{cases} \tag{12}$$

As is shown in Fig. 1, the angular frequency of γ-δ axis is ω_γ, and the difference between ω_e and ω_γ is $\Delta\omega$. In γ-δ axis, ω_γ is set to be unequal to ω_e. Due to the difference of rotation frequency between γ-δ axis and d-q axis, γ-axis scans d-axis and q-axis at a certain frequency circularly, so the γ-axis inductance (L_γ) is equal to L_q and L_d while γ-axis coincides with q-axis and d-axis respectively in a complete scan cycle.

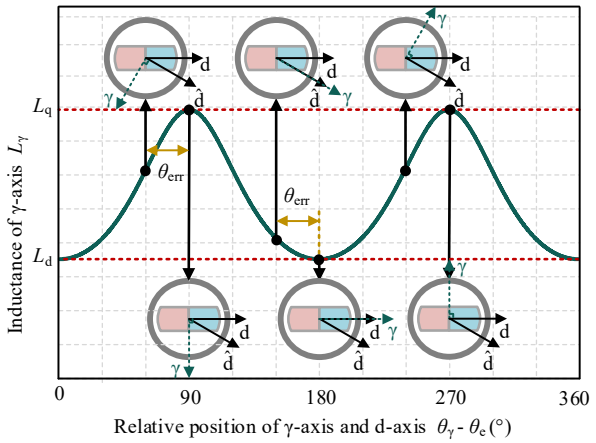

Fig. 2. Correspondence between inductance and the rotor position.

The γ-axis inductance for the transformation from the d-q axis inductances is

$$L_\gamma = L_d \cos^2\left(\theta_\gamma - \theta_e\right) + L_q \sin^2\left(\theta_\gamma - \theta_e\right) \tag{13}$$

Among all the two-phase axis systems, the d-q axis inductance matrix is a diagonal matrix, and the axial self inductance values reach their extreme, as is shown in Fig. 2. It can be seen that the rotor position error does not have an impact on the above analysis.

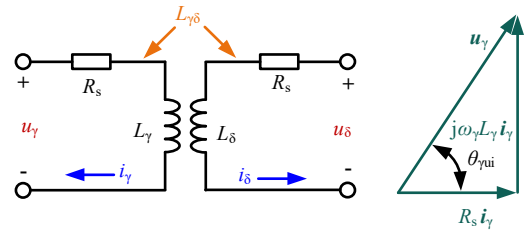

Fig. 3. Equivalent circuit and the impedance model. (a) Equivalent circuit of γ-δ axis. (b) The impedance model of γ-axis.

The equivalent circuit of γ-δ axis is shown in Fig. 3(a), where the γ-δ axis mutual inductance makes the γ-δ axis voltage equations coupled. However, if there is no external excitation signal injected into δ-axis, there will be no coupled mutual inductance term in the γ-axis voltage equation, and the γ-axis impedance model is shown in Fig. 3(b). It can be seen that the phase of $\boldsymbol{u}_\gamma$ is ahead of $\boldsymbol{i}_\gamma$, the component of $R_s\boldsymbol{i}_\gamma$ is orthogonal to $j\omega_\gamma L_\gamma \boldsymbol{i}_\gamma$, ω_γ is the angular frequency of γ-axis signals, and $\theta_{\gamma ui}$ is the angle between $\boldsymbol{u}_\gamma$ and $R_s\boldsymbol{i}_\gamma$. Therefore, L_γ can be represented as

$$L_\gamma = \frac{U_\gamma}{\omega_\gamma I_\gamma} \sin\theta_{\gamma ui} \tag{14}$$

where U_γ and I_γ are the amplitudes of $\boldsymbol{u}_\gamma$ and $\boldsymbol{i}_\gamma$ respectively.

IV. Proposed Online Inductance Identification Method

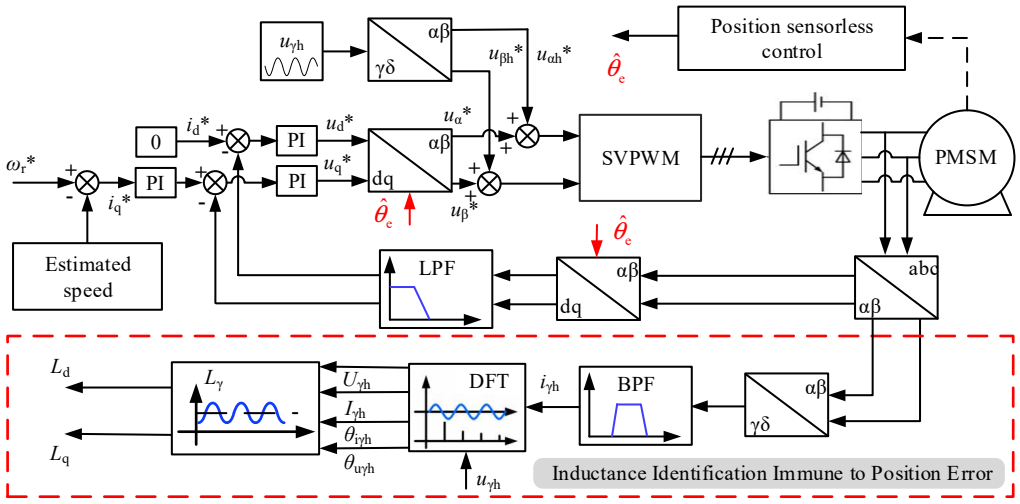

Fig. 4. Block diagram of the proposed method.

This section introduces the online PMSM inductance identification method based on HF small-amplitude voltage signal injection. The system block diagram is shown in Fig. 3.

The HF sinusoidal voltage signal injected into γ-δ-axis system can be expressed as

$$\begin{bmatrix} u_{\gamma h} \\ u_{\delta h} \end{bmatrix} = \begin{bmatrix} U_{\gamma h}\cos(\omega_h t + \theta_{\gamma h}) \\ 0 \end{bmatrix} \tag{15}$$

where $U_{\gamma h}$, ω_h, $\theta_{\gamma h}$ are the amplitude, angular frequency, and initial phase of the γ-axis injected HF voltage respectively. When transformed into d-q axis, the injected HF voltage signal can be represented as

$$\begin{bmatrix} u_{dh} \\ u_{qh} \end{bmatrix} = U_{\gamma h}\cos(\omega_h t + \theta_{\gamma h}) \begin{bmatrix} \cos(\theta_e - \theta_\gamma) \\ -\sin(\theta_e - \theta_\gamma) \end{bmatrix} \tag{16}$$

According to the impedance relationship, the expression of the high-frequency response current of d-q axis is

$$\begin{bmatrix} i_{dh} \\ i_{qh} \end{bmatrix} = \begin{bmatrix} \dfrac{U_{\gamma h}\cos(\theta_e-\theta_\gamma)\cos\theta_{dh}\cos(\omega_h t+\theta_{\gamma h}-\theta_{dh})}{\omega_h L_d} \\ \dfrac{-U_{\gamma h}\sin(\theta_e-\theta_\gamma)\cos\theta_{qh}\cos(\omega_h t+\theta_{\gamma h}-\theta_{qh})}{\omega_h L_q} \end{bmatrix} \quad (17)$$

where $\theta_{d,qh}$ are the impedance angle of HF equivalent impedance model. Considering that only $\hat{\theta}_e$ can be obtained in position sensorless control, the following will be derived based on $\hat{d}$-$\hat{q}$ axis rather than d-q axis. It will also be explained later that θ_{err} will not affect the result of PMSM inductance identification.

To ensure that the injection signal does not affect the operating conditions of PMSM, it is necessary to set a relatively high injection frequency, so the HF inductive reactance is much more than the impedance, and the impedance angle of $\theta_{d,qh}$ are considered as 90 degrees, so the expression of $i_{\gamma h}$ and L_γ can be written as

$$i_{\gamma h} = I_{\gamma h}\cos(\omega_h t+\theta_{\gamma h}-\pi/2) \quad (18)$$

$$I_{\gamma h} = \frac{U_{\gamma h}}{\omega_h}\left[\frac{\sin^2(\hat{\theta}_e+\theta_{err}-\theta_\gamma)}{L_q}+\frac{\cos^2(\hat{\theta}_e+\theta_{err}-\theta_\gamma)}{L_d}\right] \quad (19)$$

$$\begin{aligned} L_\gamma &= \frac{U_{\gamma h}}{\omega_h I_{\gamma h}} \\ &= \frac{L_d L_q}{L_q\cos^2\left(\hat{\theta}_e+\theta_{err}-\theta_\gamma\right)+L_d\sin^2\left(\hat{\theta}_e+\theta_{err}-\theta_\gamma\right)} \end{aligned} \quad (20)$$

where $I_{\gamma h}$ is the amplitude of the γ-axis HF current. It can be seen in (20) that the minimum and maximum values of L_γ are the inductance values of the accurate d-axis and q-axis respectively. Since the amplitude of the γ-axis injected HF voltage is artificially set, and the amplitude of the γ-axis HF current can be obtained by DFT algorithm, as

$$I_{\gamma h} = \frac{2}{N}\sqrt{\sum_{n=0}^{N-1}\left[i_{\gamma h}(n)\right]^2\left[\cos^2(\frac{2\pi n}{N})+\sin^2(\frac{2\pi n}{N})\right]} \quad (21)$$

where n represents the nth sampling point, N is the number of sampling points in a single operation cycle. Thus, the existence of θ_{err} will not affect the results of inductance identification in the proposed method. According to the above analysis, the identification of inductance can be completely decoupled from the rotor position error.

V. Experimental Results

In order to verify the inductance identification method proposed in this paper, the experiments were carried out on the 2.2kW IPMSM test platform, as is shown in Fig. 5. The parameters of the motor are shown in Table I.

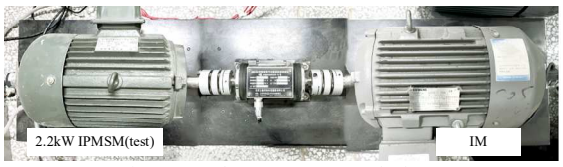

Fig. 5. 2.2kW IPMSM test platform.

TABLE I
Main Parameters of the Test IPMSM

Parameters	Values
V_{rated} [V]	380
I_{rated} [A]	5.6
n_{rated} [rpm]	1000
Pole Pairs	3
L_d [mH]	42
L_q [mH]	63
R_s [Ω]	2.75

Fig 6 shows several signals used in the PMSM inductance identification process when the motor is running with the load from no load to full load. u_γ and i_γ are the voltage and current of γ-axis respectively, including both fundamental and high frequency components, $u_{\gamma h}$ and $i_{\gamma h}$ are the γ-axis HF voltage and current respectively, processed by the band-pass filter (BPF).

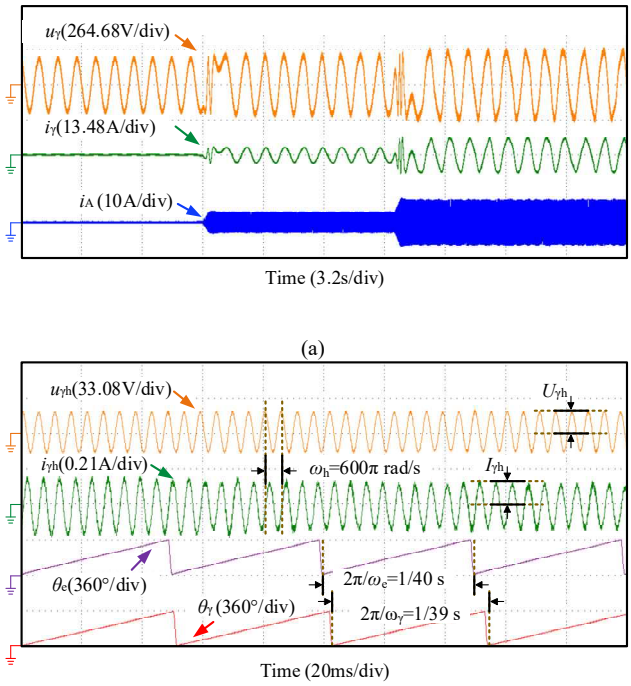

Fig. 6. Signals used in PMSM inductance identification. (a) u_γ and i_γ. (b) $u_{\gamma h}$ and $i_{\gamma h}$.

To verify the applicability of the proposed method under different motor operation conditions, position sensor is used to measure the real rotor position and manually set the different possible positions of position sensorless control.

Fig. 7 shows the PMSM inductance identification results under different PMSM load conditions and operating frequencies. The load varies by 25% of the rated-load per step from no-load to full-load, and the rotor position error is manually set to 5 degrees. Fig. 6(a) presents the experimental results at the PMSM operating frequency of 10Hz, while Fig. 6(b) presents the experimental results at the PMSM operating frequency of 20Hz.

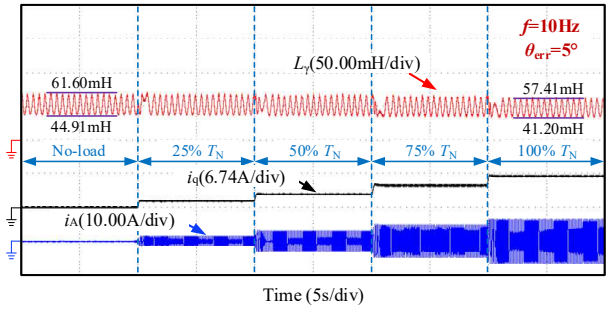

(a)

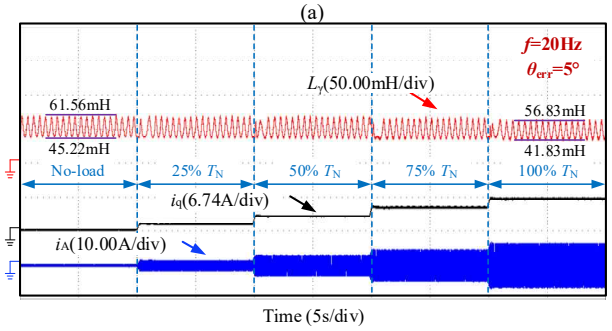

(b)

Fig. 7. Experimental results under different PMSM load conditions and operating frequencies. (a) f is 10Hz. (b) f is 20Hz.

Taking Fig 7(a) as an example, when the motor is no-load, the identification result of L_q and L_d is 61.60mH and 44.91mH respectively, the identification error is 2.22% and 6.93% respectively. As the load increases, the identification result of L_q decreases to 57.41mH, while the identification result of L_d decreases to 41.20mH. The same analysis can be performed at Fig 7(b).

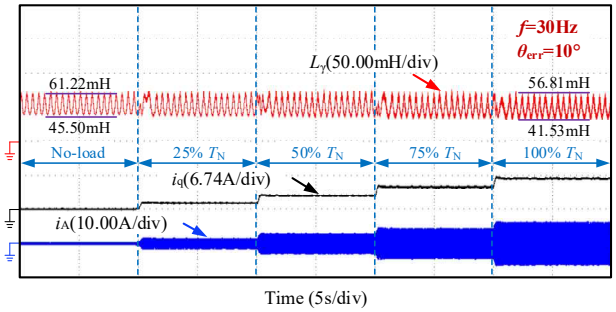

(a)

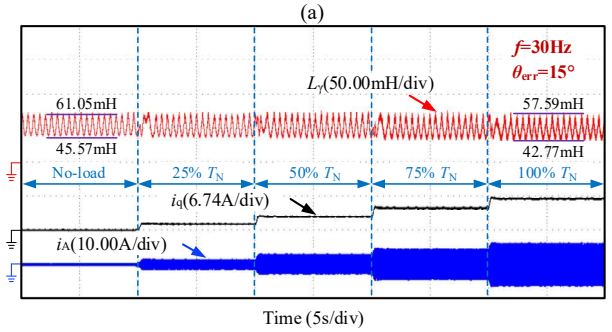

(b)

Fig. 8. Experimental results under different PMSM load conditions and rotor position errors. (a) θ_{err} is 10°. (b) θ_{err} is 15°.

Fig. 8 shows the PMSM inductance identification results under different PMSM load conditions and rotor position errors. The load varies by 25% of the rated-load per step from no-load to full-load, and PMSM operating frequency is 30Hz. Fig. 8(a) presents the experimental results when the rotor position error is manually set to 10 degrees, while Fig. 8(b) presents the experimental results when the rotor position error is manually set to 15 degrees.

TABLE II
EXPERIMENTAL RESULTS UNDER NO-LOAD CONDITION

Frequency [Hz]	Position error [°]	Result			
		L_d [mH]	Error	L_q [mH]	Error
10	5	44.91	6.93%	61.60	2.22%
20		45.22	7.67%	61.56	2.29%
30	10	45.50	8.33%	61.22	2.83%
	15	45.57	8.50%	61.05	3.10%

The inductance identification results are shown in Table II. It can be seen that the tracking effect of the results is relatively stable.

VI. CONCLUSIONS

An online inductance identification method based on HF equivalent impedance model of PMSM is proposed in this paper, which is applicable for the PMSM position sensorless control. The identification of PMSM inductance can be completely decoupled from the rotor position error by injecting the HF voltage signal into the relative rotation axis constructed in this paper, so it can be immune to the rotor position error of position sensorless control. The experimental results demonstrate that the PMSM inductance of d-q axis can be accurately identified when the rotor position error exists.

REFERENCES

[1] Q. Wang, S. Liu, G. Zhang, D. Ding, B. Li, G. Wang, and D. Xu, "Zero-Sequence Voltage Error Elimination Based Offline VSI Nonlinearity Identification for PMSM Drives," IEEE Transactions on Transportation Electrification, pp. 1-1, 2023.

[2] S. Wang, G. Zhang, Q. Wang, D. Ding, G. Bi, B. Li, G. Wang, and D. Xu, "Torque Disturbance Compensation Method Based on Adaptive Fourier-Transform for Permanent Magnet Compressor Drives," IEEE Trans. Power Electron., vol. 38, no. 3, pp. 3612-3623, Mar. 2023.

[3] X. An, G. Liu, Q. Chen, W. Zhao and X. Song, "Adjustable Model Predictive Control for IPMSM Drives Based on Online Stator Inductance Identification," in IEEE Transactions on Industrial Electronics, vol. 69, no. 4, pp. 3368-3381, April 2022.

[4] G. Wang, M. Valla, and J. Solsona, "Position Sensorless Permanent Magnet Synchronous Machine Drives—A Review," IEEE Trans. Ind. Electron., vol. 67, no. 7, pp. 5830-5842, Jul. 2020.

[5] L. Ding, Y. W. Li and N. R. Zargari, "Discrete-Time SMO Sensorless Control of Current Source Converter-Fed PMSM Drives with Low Switching Frequency," in IEEE Transactions on Industrial Electronics, vol. 68, no. 3, pp. 2120-2129, March 2021.

[6] H. Li, Z. Wang, C. Wen and X. Wang, "Sensorless Control of Surface-Mounted Permanent Magnet Synchronous Motor

Drives Using Nonlinear Optimization," in IEEE Transactions on Power Electronics, vol. 34, no. 9, pp. 8930-8943, Sept. 2019.
[7] L. Qu, W. Qiao and L. Qu, "An Enhanced Linear Active Disturbance Rejection Rotor Position Sensorless Control for Permanent Magnet Synchronous Motors," in IEEE Transactions on Power Electronics, vol. 35, no. 6, pp. 6175-6184, June 2020.
[8] G. Feng, C. Lai, X. Tan, W. Peng and N. C. Kar, "Multi-Parameter Estimation of PMSM Using Differential Model with Core Loss Compensation," in IEEE Transactions on Transportation Electrification, vol. 8, no. 1, pp. 1105-1115, March 2022.
[9] Y. Inoue, Y. Kawaguchi, S. Morimoto and M. Sanada, "Performance Improvement of Sensorless IPMSM Drives in a Low-Speed Region Using Online Parameter Identification," in IEEE Transactions on Industry Applications, vol. 47, no. 2, pp. 798-804, March-April 2011.
[10] G. Feng, C. Lai, K. Mukherjee and N. C. Kar, "Current Injection-Based Online Parameter and VSI Nonlinearity Estimation for PMSM Drives Using Current and Voltage DC Components," in IEEE Transactions on Transportation Electrification, vol. 2, no. 2, pp. 119-128, June 2016.
[11] C. Wu, Y. Zhao and M. Sun, "Enhancing Low-Speed Sensorless Control of PMSM Using Phase Voltage Measurements and Online Multiple Parameter Identification," in IEEE Transactions on Power Electronics, vol. 35, no. 10, pp. 10700-10710, Oct. 2020.
[12] M. N. Uddin and M. M. I. Chy, "Online Parameter-Estimation-Based Speed Control of PM AC Motor Drive in Flux-Weakening Region," in IEEE Transactions on Industry Applications, vol. 44, no. 5, pp. 1486-1494, Sept.-Oct. 2008.
[13] S. J. Underwood and I. Husain, "Online Parameter Estimation and Adaptive Control of Permanent-Magnet Synchronous Machines," in IEEE Transactions on Industrial Electronics, vol. 57, no. 7, pp. 2435-2443, July 2010.
[14] Z. -H. Liu, H. -L. Wei, Q. -C. Zhong, K. Liu and X. -H. Li, "GPU Implementation of DPSO-RE Algorithm for Parameters Identification of Surface PMSM Considering VSI Nonlinearity," in IEEE Journal of Emerging and Selected Topics in Power Electronics, vol. 5, no. 3, pp. 1334-1345, Sept. 2017.
[15] Z. -H. Liu, H. -L. Wei, Q. -C. Zhong, K. Liu, X. -S. Xiao and L. -H. Wu, "Parameter Estimation for VSI-Fed PMSM Based on a Dynamic PSO With Learning Strategies," in IEEE Transactions on Power Electronics, vol. 32, no. 4, pp. 3154-3165, April 2017.
[16] Q. Wang, G. Wang, N. Zhao, G. Zhang, Q. Cui and D. Xu, "An Impedance Model-Based Multiparameter Identification Method of PMSM for Both Offline and Online Conditions," in IEEE Transactions on Power Electronics, vol. 36, no. 1, pp. 727-738, Jan. 2021.